geoconvention
Virtual Event
September 21-23
2020
CSPG • CSEG • CWLS • GAC • MAC • IAH

Optimum offset range and source-receiver orientations for detecting the Sv-P converted waves in anisotropic media

Hossein, Jodeiri Akbari Fam[1], Mostafa, Naghizadeh[1], Navid, Shadmanaman[2]
[1] Mineral Exploration Research Centre, Harquail School of Earth Sciences, Goodman School of Mines, Laurentian University, [2] Faculty of Mining Engineering, Sahand University of Technology

Summary

Shear (S) wave information is important in seismic interpretation and reservoir characterization studies. Due to the high cost and technical difficulties in recording full elastic seismic data (3D-9C), utilizing converted Sv-P waves can help to extract S-wave information. Analysis of amplitude and phase variations of converted waves versus offset/angle is useful for the identification of converted wave reflections in the seismic sections. We study the energy distribution of Sv-P waves arriving at various incidence angles and different Vp/Vs ratios using Zoeppritz equations and seismic source radiation patterns. Next, using forward modeling and ray tracing methods, we obtained the source and receiver orientations necessary to record Sv-P waves with distinguishable energies. The Sv-P conversion mode often occurs before the critical angle which corresponds to large source-receiver offsets. Depending on the target depth, the mid/far-offset data are necessary for the optimal recording of the Sv-P reflections. Therefore, using an appropriate acquisition design, the Shear velocity information can be derived from conventional (vertical-vertical) seismic data.

Introduction

Shear (S) wave information plays a key role in exploration, geomechanical modeling, and reservoir analysis. One can obtain the S-wave properties using converted waves recorded on the seismic data (Stewart et al., 2004; Hardage et al., 2014; DeAngelo and Hardage, 2016). The processing of the seismic converted wave is one of the challenging tasks in the industry and it requires its own velocity analysis, static, and move-out corrections. Recognizing the amplitude of the converted wave in different reflection angles is an essential pre-processing step for designing an optimal seismic acquisition, processing algorithm, and interpretation (Jodeiri Akbari Fam and Shadmanaman, 2018).
The study of elastic body wave propagation theory shows that vertical sources not only generate P waves, but also do have the ability to produce S waves which lead to four reflective waves: P-P, P-Sv, Sv-Sv, and Sv-P (Hardage et al., 2014). This has been approved by Hardage and Wagner (2014) based on the analyses of a walk-away VSP survey seismic data acquired by a single vertical vibrator. By analyzing 2D-3C real near-surface seismic data sets, Pugin and Yilmaz (2017) have shown that there is no “pure P” land-based vertical source. Also, Hardage and Wagner (2018) used finite-difference modeling to generate direct-P and direct-Sv radiation produced by vertical sources in real seismic field conditions (propagation media). Their results indicate that vertical sources produce S wavefield that is appropriate for imaging even for deep geologic targets. Gaiser (2019) has modeled S-wave radiation in isotropic and anisotropic media.
In this study, we modeled the radiation pattern of vertical source for consolidated and unconsolidated media to examine the distribution of S- and P-waves in different radiation angles. Next, we computed the partitioning of produced seismic wave energy at interfaces with different properties. Then, the final reflection energy of P-P and Sv-P waves have been evaluated. To determine the optimal offsets and source and receiver orientations with considerable Sv-P wave energy, we simulated various scenarios over several synthetic velocity models.

Theory

In this study, we combine the amplitude of direct-P and direct-S waves generated by a vertical source at a free-surface with reflection partitioning of P-P and Sv-P across a solid-solid interface for isotropic and anisotropic media. The Zoeppritz equations (Zoeppritz 1919) provide the reflection and transmission coefficients for plane waves which depend on elastic parameters on each side of the reflecting interface in isotropic media. In 1992, Graebner had published exact solutions of amplitude partitioning for anisotropic VTI media. In these formulas (Aki and Richards, 1980), it has been assumed that incident energy is uniformly distributed (unit amplitude) for all incident angles (like a point source radiating spherical waves) which is not a realistic assumption. We compute the distribution of the P-P and Sv-P reflection energies as a function of the incidence angle by considering the radiation pattern of the seismic waves as the incident (illuminated) energies to the interface. Miller and Pursey (1953) and Gaiser (2019) derived the equations for P- and S-radiation patterns produced by vertical force at the earth's surface with isotropic and anisotropic media, respectively.

For an isotropic medium, we derive the P-P and Sv-P energy coefficients (and) by considering the direct-P and direct-S as the down-going incident wave generated by a vertical source. These equations are expressed as follows:

$$E_{PP}^{iso}=U_{P}^{iso}.\left|R_{PP}^{iso}\right|,$$

$$E_{PP}^{iso}=\frac{q_{P1}.\left(q_{S1}^{2}-p^{2}\right)}{V_{P1}.\left[\left(q_{S1}^{2}-p^{2}\right)^{2}+4\,p^{2}.q_{P1}.q_{S1}\right]}.\left|\frac{\left[\left(b.q_{P1}-c.q_{P2}\right).F-\left(a+d.q_{P1}.q_{S2}\right).H.p^{2}\right]}{D}\right|, \quad (1)$$

$$E_{SP}^{iso}=U_{Sv}^{iso}.\left|R_{SP}^{iso}\right|.\frac{V_{P1}.\cos i_{1}}{V_{S1}.\cos j_{1}},$$

$$E_{SP}^{iso}=\frac{2\,p.q_{P1}.q_{S1}}{V_{S1}.\left[\left(q_{S1}^{2}-p^{2}\right)^{2}+4\,p^{2}.q_{P1}.q_{S1}\right]}.\left|\frac{2q_{S1}\left[a.b+c.d.q_{P2}.q_{S2}\right]p.V_{S1}}{\left(V_{P1}.D\right)}\right|.\frac{V_{P1}.\cos i_{1}}{V_{S1}.\cos j_{1}}, \quad (2)$$

where U_{P}^{iso} and U_{Sv}^{iso} are the displacement amplitude for P- and Sv-wave radiations in an isotropic medium, $R_{PP}^{iso}$and R_{SP}^{iso} are the P-P and Sv-P reflection coefficients. [V_{P1}, V_{S1}, ρ_1] and [V_{P2}, V_{S2}, ρ_2] denote first and second half-space elastic parameters, respectively. In equation (1) and (2), p is the P-wave ($p_P=\sin i_1/V_{P1}$) and Sv-wave ($p_S=\sin j_1/V_{S1}$) horizontal slowness, respectively. q_{P1} and q_{P2} are P-wave reflected and refracted downgoing vertical slowness and q_{S1} and q_{S2} are S-wave reflected and refracted downgoing vertical slowness, respectively.

$$a=\rho_2\left(1-2V_{S2}^{2}p^{2}\right)-\rho_1\left(1-2V_{S1}^{2}p^{2}\right), \qquad \cos i_1=\sqrt{1-V_{P1}^{2}.p^{2}}, \qquad E=b.q_{P1}+c.q_{P2},$$

$$b=\rho_2\left(1-2V_{S2}^{2}p^{2}\right)-2\rho_1\left(V_{S1}^{2}p^{2}\right), \qquad \cos i_2=\sqrt{1-V_{P2}^{2}p^{2}}, \qquad F=b.q_{S1}+c.q_{S2},$$

$$c=\rho_1\left(1-2V_{S1}^{2}p^{2}\right)+2\rho_2\left(V_{S2}^{2}p^{2}\right), \qquad \cos j_1=\sqrt{1-V_{S1}^{2}.p^{2}}, \qquad G=a-d.q_{P1}.q_{S2},$$

$$d=2\left(\rho_2V_{S2}^{2}-\rho_1V_{S1}^{2}\right), \qquad \cos j_2=\sqrt{1-V_{S2}^{2}p^{2}}, \qquad H=a-d.q_{P2}.q_{S1},$$

$$q_{P1}=\sqrt{\frac{1}{V_{P1}^{2}}-p^{2}},q_{P2}=\sqrt{\frac{1}{V_{P2}^{2}}-p^{2}}, \qquad q_{S1}=\sqrt{\frac{1}{V_{S1}^{2}}-p^{2}},q_{S2}=\sqrt{\frac{1}{V_{S2}^{2}}-p^{2}}, \qquad D=E.F+G.H.p^{2}.$$

where, i_1, i_2, j_1, and j_2 are incident or reflected P-wave, transmitted P-wave, incident or reflected S-wave, and transmitted S-wave angles with respect to the vertical axis, respectively. For a weakly anisotropic VTI media, we modified and corrected Graebner's approach to calculate the reflection

coefficients (Graebner, 1992). The P-P and Sv-P energy coefficients (E_{PP}^{aniso} and E_{SP}^{aniso}) are expressed as follows:

$$E_{PP}^{aniso} = U_{P}^{aniso} . \left| R_{PP}^{VTI} \right|, \tag{3}$$

$$E_{SP}^{aniso} = U_{Sv}^{aniso} . \left| R_{SP}^{VTI} \right| . \frac{V_{P1}(\theta) . \cos i_1(\theta)}{V_{S1}(\theta) . \cos j_1(\theta)}, \tag{4}$$

where U_{P}^{aniso} and U_{Sv}^{aniso} are the displacement amplitude for P- and Sv-wave radiations in a VTI medium, R_{PP}^{VTI} and R_{SP}^{VTI} are the P-P and Sv-P reflection coefficients (for detail see Graebner, 1992; Tsvankin, 2012; Gaiser, 2019). $V_P(\theta)$ and $V_S(\theta)$ are the P and Sv phase velocities and θ is the phase angle. We used the exact phase velocity and phase angle, while Gaiser has used approximation solutions. The displacement directions and reflection coefficients are defined in group velocity directions.

Vertical Source Radiation patterns

Figures 1 and 2 show the 3D radiation patterns of the P- and Sv-wave energies produced by a land-based vertical source applied to a homogeneous half-space with different poison ratios for isotropic and weakly anisotropic VTI media, respectively. Figures 3 and 4 show a constant azimuth vertical slice of the 3D radiation pattern in Figures 1 and 2, respectively. The semi circulars in Figures 3 and 4 depict the propagated amplitude and the radial lines show the takeoff angles relative to the vertical axis.

a) b)

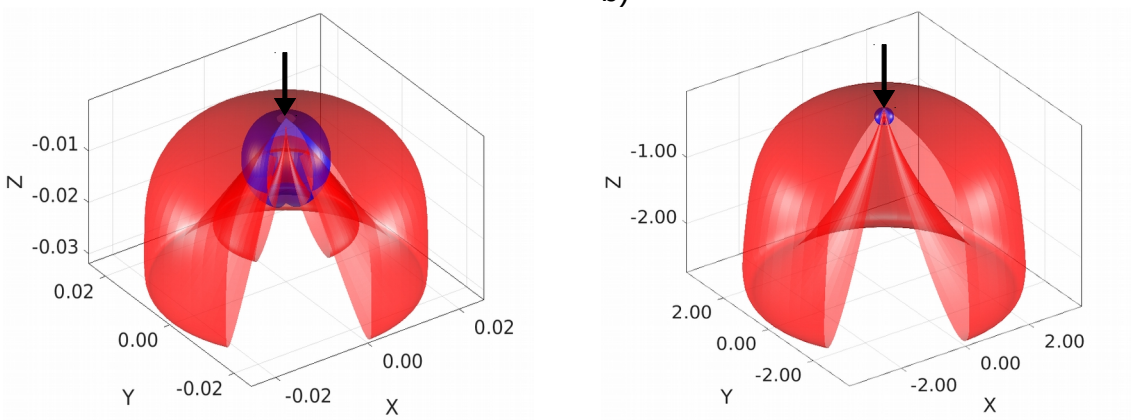

Figure 1: 3D radiation patterns of the P (blue) and Sv (red) waves energies produced by a land-based vertical source applied to the isotropic half-space, a) consolidate (V_{P1}/V_{S1} = 1.75 and υ_1 = 0.26) and b) unconsolidate (V_{P1}/V_{S1} = 4 and υ_1 = 0.47).

a) b)

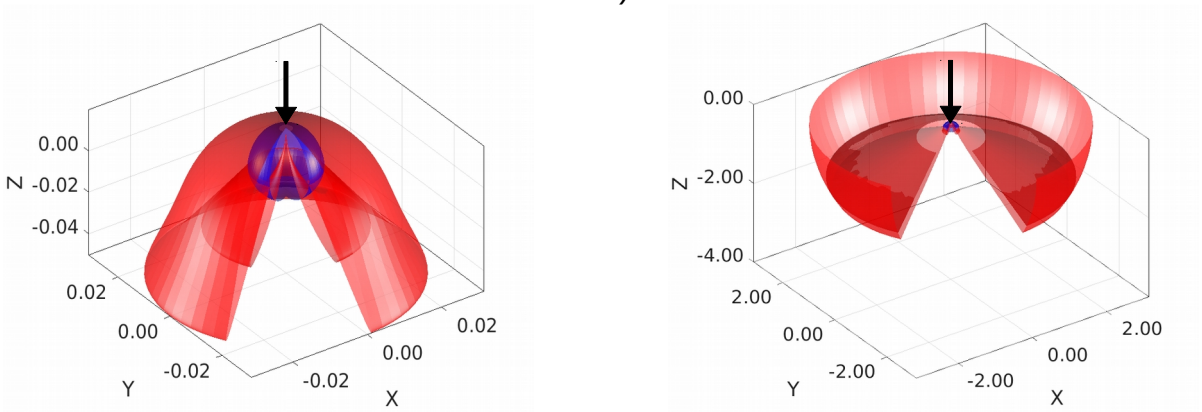

Figure 2: 3D radiation patterns of the P (blue) and Sv (red) waves energies produced by a land-based vertical source applied to the weakly anisotropic VTI half-space, a) consolidate (V_{P1}/V_{S1} = 1.75 and υ_1 = 0.26) and b) unconsolidate (V_{P1}/V_{S1} = 4 and υ_1 = 0.47).

a) b)

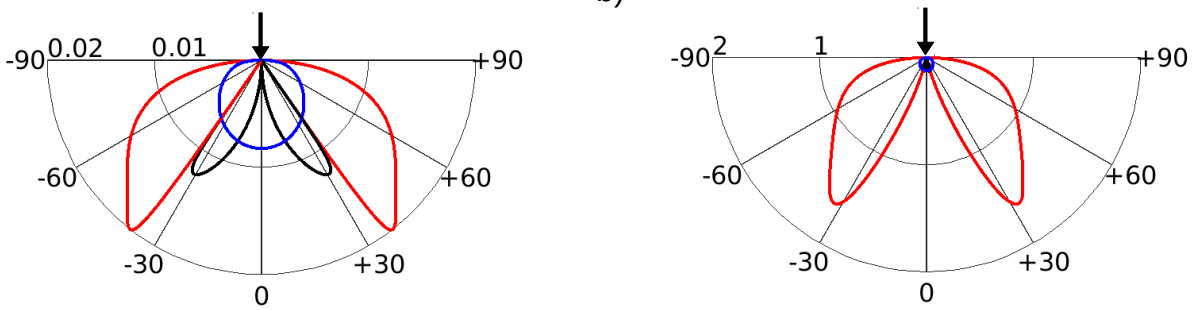

Figure 3: 2D radiation patterns of the P (blue) and Sv (red+black) waves energies produced by a land-based vertical source applied to the isotropic a) consolidated and b) unconsolidated half-space.

a) b)

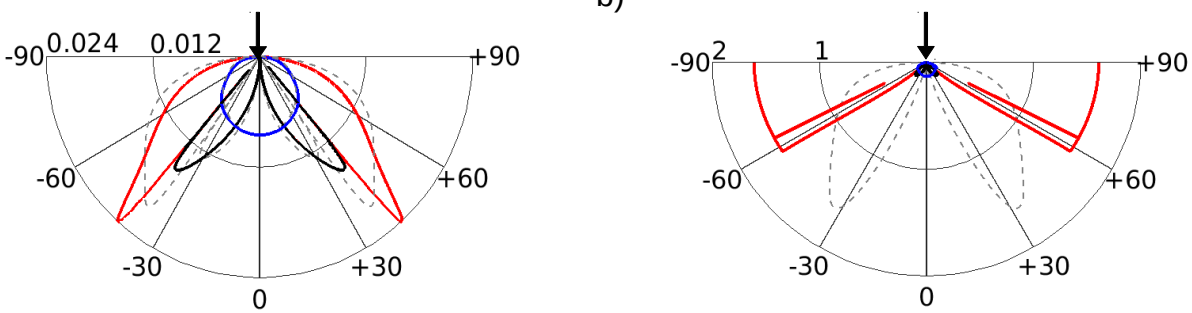

Figure 4: 2D radiation patterns of the P (blue) and Sv (red+black) waves energies produced by a land-based vertical source applied to the weakly anisotropic VTI a) consolidated and b) unconsolidated half-space. Gray dashed lines are the 2D radiation patterns for the isotropic medium.

Seismic energy distribution at layered interfaces

We examined our proposed formulation on four different synthetic geological models. Models 1 and 2 include an unconsolidated media (V_{P1}/V_{S1}=4) over a half-space with low (V_{P2}/V_{P1}=1.5) and high (V_{P2}/V_{P1}=2.5) impedance contrasts, respectively. For models 3 and 4, the first medium is consolidated medium (V_{P1}/V_{S1}=4) and the second layer is a half-space with low and high impedance contrasts (Table 1).

Table 1: Synthetic Models' properties *(ρ (kg/m^3)* and *V(m/s)*).

	First Layer					Second Layer				
	V_{P1}	V_{S1}	ρ_1	ϵ_1	δ_1	V_{P2}	V_{S2}	ρ_1	ϵ_2	δ_2
Model 1	600	150	1800	0.125	0.025	900	514.3	2000	0.25	0.05
Model 2						1500	857.2	2200	0.25	0.05
Model 3	2000	1142.9	2400	0.25	0.15	3000	1714.3	2700	0.5	0.3
Model 4						50000	2857.1	3000	0.5	0.3

Figures 5a-5d show the final reflected energy of different take-off angles for isotropic models 1-4 in Table 1 after taking into account the radiation patterns that were shown in Figure 3. Notice that in the unconsolidated media, due to the high amplitude of S waves, the propagated P wave has a very low amplitude, and the P wave radiation pattern is not well pronounced. In this case, a significant part of the radiated direct-S wave contributes to the generation of the surface waves (Figure 3b). Figures 6a-6d show the final reflected energy of different take-off angles for weakly anisotropic VTI models 1-4 in Table 1 after taking into account the radiation patterns that were shown in Figure 4.

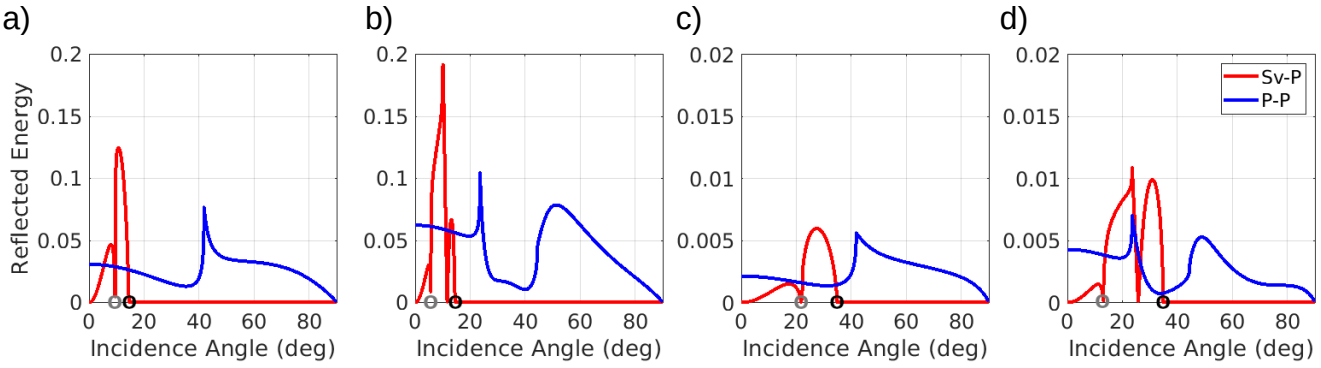

Figure 5: Reflected energy coefficient of P-P (blue) and Sv-P (red) waves for isotropic a) model 1, b) model 2, c) model 3, and d) model 4. Gray and black open circles represent the critical angles for the transmitted and reflected converted Sv-P waves.

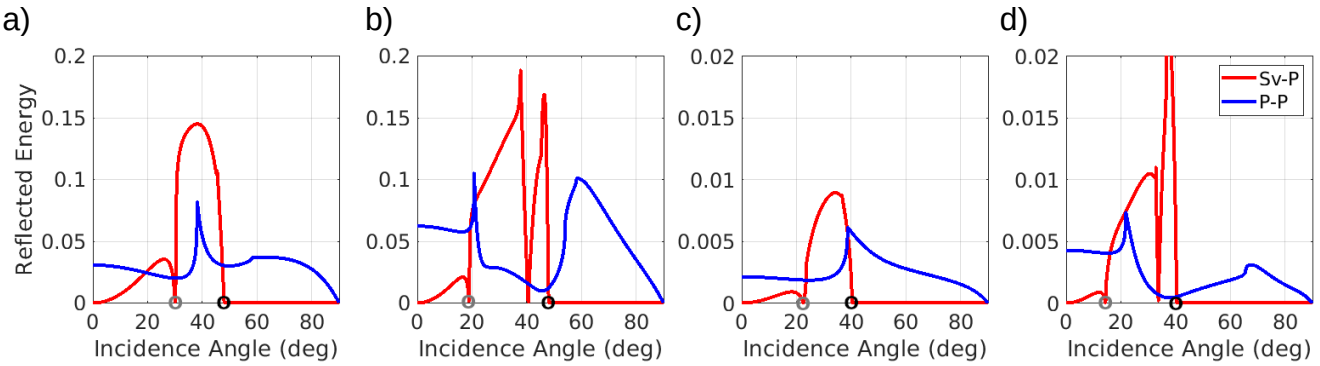

Figure 6: Reflected energy coefficient of P-P (blue) and Sv-P (red) waves for weakly anisotropic VTI a) model 1, b) model 2, c) model 3, and d) model 4. Gray and black open circles represent the critical angles for the transmitted and reflected converted Sv-P waves.

We computed the critical angles for each model (Table 2). These angles depend on the velocity ratios and valid for the aforementioned models. It gives us a general point of view about the incident angles, that Sv-P converted wave reflects significantly. In Figures 5 and 6, $\theta_1=\sin^{-1}\left(V_{S1}/V_{P2}\right)$ and $\theta_2=\sin^{-1}\left(V_{S1}/V_{P1}\right)$ have been indicated with black and gray open circles, respectively.

Table 2: The critical angles for the Sv-P converted waves

	S-incident wave (Isotropic media)		S-incident wave (Anisotropic media)	
Critical Angle	$\theta_1=\sin^{-1}\left(V_{S1}/V_{P2}\right)$	$\theta_2=\sin^{-1}\left(V_{S1}/V_{P1}\right)$	$\theta_1=\sin^{-1}\left(V_{S1}/V_{P2}\right)$	$\theta_2=\sin^{-1}\left(V_{S1}/V_{P1}\right)$
Model 1	9.59	14.48	30.02	48.01
Model 2	5.74	14.48	18.91	48.01
Model 3	22.39	34.85	22.46	40.39
Model 4	13.21	34.85	14.32	40.39

The effects of V_P/V_S velocity ratio

We have investigated the effects of V_P/V_S velocity ratios on the final reflected energy for model 3 (Figure 7). By increasing V_P/V_S ratios, the amplitude of the recorded P-P mode increases while the amplitude of the Sv-P mode decreases. Also, in the isotropic media, the optimal incident angles (and consequently the optimal offsets) for maximum reflection amplitude of Sv-P converted modes are reduced and limited to smaller angles. However, in the VTI media with ($\epsilon_1-\delta_1\geqslant 0.1$), by increasing the V_P/V_S ratios with constant Thomsen parameters (ϵ and δ), the optimal incident angles were increased.

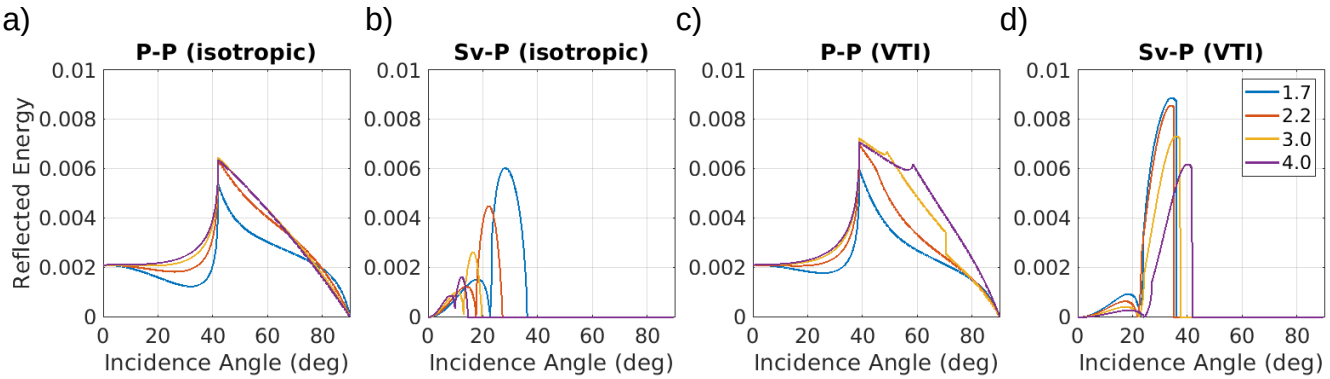

Figure 7: Final reflected energy coefficients for different V_P/V_S ratios for model 3 a) P-P (isotropic), b) Sv-P (isotropic), c) P-P (VTI), and d) Sv-P (VTI).

Synthetic model

Using the ray-tracing method, we simulated the Sv-P converted data with horizontal/vertical sources and single-component receivers over a layered cake synthetic model (profile length=10000m, number of receivers=400, receiver interval=25m). Figure 8 shows the Sv-P amplitude versus offset graph for the first, fifth, and ninth interfaces. The first column shows the energy partitioning at the layer boundaries. The second column depicts the reflected energy by considering the effect of the radiation pattern. The third and fourth columns are the recorded amplitude of Sv-P waves generated by the horizontal and vertical sources, respectively. HH and HV represent the modes generated by a horizontal source and recorded by horizontal and vertical receivers, respectively. Similarly, VH and VV represent the modes generated by a vertical source and recorded by horizontal and vertical receivers, respectively.

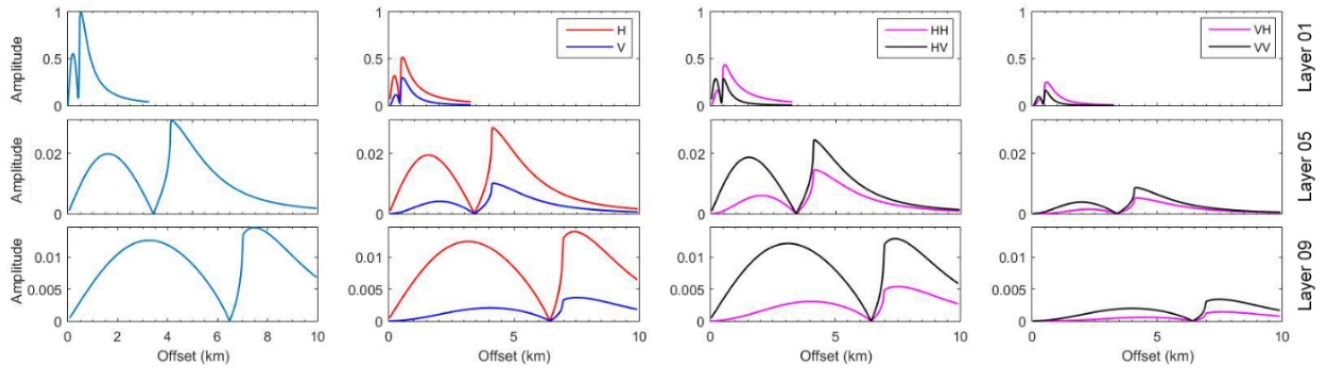

Figure 8: The Sv-P wave amplitude versus offset for first, fifth, and ninth interfaces.

Conclusions

Numerical modeling has shown that Sv-P converted waves have a measurable amplitude (even more than P-P reflection data in particular offsets) in conventional seismic data generated by the vertical source and recorded by vertical receivers (vertical-vertical). This study approved that vertical-vertical seismic data configuration does not only have P-P reflection data but also has detectable Sv-P waves. Consequently, the shear wave information can be potentially extracted from vertical-vertical seismic data without using a three-component (3C) data set. Analysis of the reflection angle indicates that the Sv-P energy is limited by the critical angle of $\theta_2 = \sin^{-1}\left(V_{S1}/V_{P1}\right)$ and we can't expect to record them at the larger incidence angles. Also, the energy conversion ratio of Sv into P mode depends on the velocity ratios of media and Sv-P conversion mode only occurs between zero and this incidence angle. The highest Sv-P energy conversion ratio mainly occurs between the incident angles of $\theta_1 = \sin^{-1}\left(V_{S1}/V_{P2}\right)$ and $\theta_2 = \sin^{-1}\left(V_{S1}/V_{P1}\right)$, which corresponds to the mid/far-offset data. For the VTI media with ($\epsilon_1 - \delta_1 \geqslant 0.1$ and $\epsilon_2 \geqslant 2\epsilon_1$), the optimal subsurface condition for detecting the Sv-P mode on a wider offset range is an unconsolidated overburden layer which has a high impedance contrast with the underlying layer. Also, the unconsolidated overburden makes the arrival angle of the reflected energy to be near vertical and detectable on vertical receivers.

Acknowledgements

This research was funded by the NSERC Canada First Research Excellence Fund (MERC-ME-2020-048).

References

Aki, K., and Richards, P. G., 1980, Quantitative seismology: Theory and methods: New York.

De Angelo, M.V. and Hardage, B.A., 2016, Comparing PP, P-SV, and SV-P mode waves in the Midland Basin. West Texas: Interpretation, 4, no. 2, T183–T190.

Gaiser, J., 2019, Modelling S-wave radiation for SP-waves in isotropic and anisotropic media: Geophysical Prospecting, 67, no. 9, 2414-2431.

Graebner, M., 1992, Plane-wave reflection and transmission coefficients for a transversely isotropic solid. *Geophysics*, *57*(11), 1512-1519.

Hardage, B., Sava, D., and Wagner, D., 2014, SV-P: An ignored seismic mode that has great value for interpreters: Interpretation, 2, no. 2, SE17-SE27.

Hardage, B.A. and Wagner, D., 2014, Generating direct-S modes with simple, low-cost, widely available seismic sources: Interpretation, 2(2), pp.SE1-SE15.

Hardage B.A. and Wagner D., 2018, Direct-SV radiation produced by land-based P-sources – Part 1: Surface sources: Interpretation 6, T569–T584.

Jodeiri Akbari Fam, H. and Shadmanaman, H., 2018, Modeling of amplitude and phase variations of converted waves versus offset and VP/VS ratio: Iranian Journal of Geophysics, 11, no. 4, 67-62.

Miller, G. and Pursey, H., 1954, The field and radiation impedance of mechanical radiators on the free surface of a semi-infinite isotropic solid: In Proceedings of the Royal Society of London A: Mathematical, Physical and Engineering Sciences, 521-541.

Pugin, A. and Yilmaz, O., 2017, There is no pure P-or S-wave land seismic source: 87th Annual International Meeting, SEG, Expanded Abstracts, 5162-5166, doi: 10.1190/segam2017-17650931.1.

Stewart, R.R., Gaiser, J.E., Brown, R.J. and Lawton, D.C., 2003, Converted-wave seismic exploration: Applications: Geophysics, 68, no. 1, 40-57.

Tsvankin I., 2012, Seismic Signatures and Analysis of Reflection Data in Anisotropic Media: Society of Exploration Geophysicists.

Zoeppritz, K., 1919, Über reflexion und durchgang seismischer Wellen durch Unstetigkerlsfläschen: Uber Erdbedbenwellen VII B. Nachrichten der Königlichen Gesellschaft der wissenschaften zu Göttingen: Mathematish-physkalishe Klasse, K1, 57–84 (in German).